Charge Carrier Cooling Bottleneck Opens Up Nonexcitonic Gain Mechanisms in Colloidal CdSe Quantum Wells

Tomar, Renu; Kulkarni, Aditya; Chen, Kai; Singh, Shalini; Van Thourhout, Dries; Hodgkiss, Justin M.; Siebbeles, Laurens D.A.; Hens, Zeger; Geiregat, Pieter

Citation (APA)
Tomar, R., Kulkarni, A., Chen, K., Singh, S., Van Thourhout, D., Hodgkiss, J. M., Siebbeles, L. D. A., Hens, Z., & Geiregat, P. (2019). Charge Carrier Cooling Bottleneck Opens Up Nonexcitonic Gain Mechanisms in Colloidal CdSe Quantum Wells. *Journal of Physical Chemistry C*, *123*(14), 9640-9650. https://doi.org/10.1021/acs.jpcc.9b02085

Important note
To cite this publication, please use the final published version (if applicable).
Please check the document version above.

A Charge Carrier Cooling Bottleneck Opens up Non-Excitonic Gain Mechanisms in Colloidal CdSe Quantum Wells

Renu Tomar,[†,‡] Aditya Kulkarni,[¶] Kai Chen,[§,∥,⊥] Shalini Singh,[†,‡] Dries van Thourhout,[#,‡] Justin M. Hodgkiss,[§,∥,⊥] Laurens D.A. Siebbeles,[¶] Zeger Hens,[†,‡] and Pieter Geiregat[*,†,‡]

†*Physics and Chemistry of Nanostructures, Ghent University, Ghent, 9000, Belgium*
‡*Center for Nano and Biophotonics, Gent, 9000, Belgium*
¶*Optoelectronic Materials Section, Department of Chemical Engineering, Delft University of Technology, Van der Maasweg 9, 2629HZ, Delft, The Netherlands*
§*The MacDiarmid Institute for Advanced Materials and Nanotechnology, Wellington, 6012, New Zealand*
∥*School of Chemical and Physical Sciences, Victoria University of Wellington, Wellington, 6012, New Zealand*
⊥*The Dodd-Walls Centre for Photonic and Quantum Technologies, Wellington, 6012, New Zealand*
#*Photonics Research Group, Department of Information Technology, Ghent University, Ghent, 9000, Belgium*

E-mail: Pieter.Geiregat@Ugent.be

Abstract

Ultrathin two-dimensional (2D) materials have received much attention in the past years for a wide variety of photonic applications due to their pronounced room temperature excitonic features, leading to unique properties in terms of light-matter interaction. However, only a few studies focus on light amplification and the complex photo-physics at high excitation density. The beneficial nature of strong excitonic effects on optical gain remain hence unquantified and, despite the increased binding energies of the excitonic species, it remains unclear what the involvement of 2D excitons would be in optical gain. Here, we use colloidal CdSe nanoplatelets as a model system for colloidal 2D materials and show, using a quantitative and combinatory approach to ultrafast spectroscopy, that several excitation density-dependent optical gain regimes exist. At low density, optical gain originates from excitonic molecules delivering large material gains up to 20.000 cm^{-1} with an Auger limited lifetime of a few hundred picoseconds. At increasing pair density, we observe a persistence of this excitonic gain regime and the unexpected co-existence of blue-shifted and significantly enhanced optical gain up to 10^5 cm^{-1}. We show that this peculiar situation originates from a carrier cooling bottleneck at high density that limits further exciton formation from unbound charge carriers. The insulating (multi-)exciton gas is found to co-exist with the conductive phase, indicating the absence of a full Mott transition. Our results shed a new light on the photo-physics of excitons in strongly excited 2D materials and pave the way for the development of more efficient (broadband) optical gain media and/or high exciton density applications.

1 Introduction

Two-dimensional (2D) materials are considered as prime candidates for realizing low-cost and tunable optoelectronic devices.[1,2] Applications in fields as diverse as light emission, photodetection and quantum optics can make use of the distinct and high-oscillator strength excitonic transitions and/or the tunable, narrow photoluminescence found in such materials

at room temperature.[3–5] Recent years saw an increase in the number of available inorganic 2D materials such as transition metal dichalcogenide monolayers,[3] layered perovskites[6] and II-VI nanoplatelets.[7] The strong Coulomb correlations leading to stable and strong excitonic features might be very beneficial for increasing the light-matter interactions required for large and/or low threshold optical gain. Several reports indicated for example low-threshold lasing using 2D materials.[8,9] However, since net modal gain only develops at very high carrier densities, the possible role of those exciton(s) (complexes) in the process remains unclear.[10–12] Indeed, within a mass-action model excitons - and higher complexes such as excitonic molecules - only form when the associated binding energy and pair density is sufficiently large. On the other hand, it is well-known that 2D excitons dissociate more readily to form unbound carriers at high excitation density. This effect is due to the density-induced screening of the attractive Coulomb interactions which reduces the exciton binding energy, leading to so-called Mott transitions and overall intricate phase diagrams between insulating excitonic species and unbound charge carriers.[10,11,13] Optical gain in epitaxially grown quantum wells, for example, is mostly mediated by an electron-hole plasma, even at cryogenic temperatures.[14] Given the exceptionally large binding energy of excitons in colloidal 2D materials, in large due to reduced screening,[15] it is not clear to what extent these concepts still hold.[16,17] As one of the few quantitative reports on the optical gain mechanism in 2D materials, Chernikov *et al.* observed a strong band-gap renormalization and transition to an unbound electron-hole plasma in WS_2 at high carrier density associated with the development of gain.[18] This observation is remarkable given the large binding energies (> 300 meV) for the 2D excitons.[19]

It is clear that quantitative studies on optical gain are therefore much needed in order to assess the relation between stimulated emission and the complex mixture of carrier types that exists in strongly excitonic 2D materials at high density, such as 2D excitons, excitonic molecules and free charges.

CdSe 2D nanoplatelets, also called colloidal quantum wells, provide an excellent test-bed

for this purpose as they can be obtained as scatter-free colloidal dispersions with high luminescence quantum yield and excellent colloidal stability.[7,20] Several reports have demonstrated excellent light amplification properties using these colloidal quantum wells, such as large modal gains up to 500 cm^{-1} and low lasing thresholds down to tens of $\mu J/cm^2$, pointing towards a seemingly huge potential of these materials.[8,21–25] Apart from core only CdSe platelets, also more complex architectures have been studied such as core/shell and core/crown systems.[26,27] The development of optical gain in CdSe (-based platelets was however studied mainly through thin-film measurements, where either amplified spontaneous emission (ASE) or lasing was employed.[28,29] Unfortunately, such approaches fail to elucidate the fundamentals of the gain mechanism, *i.e.* which type of interactions and excitations (free charge carriers, excitons, ...) are required to achieve net optical gain. Nor do they provide any prospect on the full potential of the material as the measured properties are inherently linked to the development of net stimulated emission dictated by the film and/or cavity losses.[25] A case in point here is the alleged threshold for stimulated emission, where energy densities (typically in $\mu J/cm^2$) are reported instead of generated excitation densities. Although energy densities have a high practical value, the density of carriers, *i.e.* the number of absorbed photons, is the most relevant parameter for a proper mechanistic understanding of optical gain in this unique class of materials. Nanoplatelets can be deceptive in this respect, as they offer larger intrinsic absorption coefficients at short wavelengths due to a reduced in-plane screening.[30]

Herein, we report on an extensive quantitative study of optical gain development and the associated high excitation density photo-physics of colloidal 2D CdSe quantum wells. By combining a comprehensive set of femtosecond transient absorption, photoluminescence and terahertz spectroscopy, we were able to identify different optical gain regimes and a remarkable absence of a clear exciton Mott transition. At low electron-hole pair densities, a gain band appears at the low energy side of the heavy-hole exciton absorption that was assigned to stimulated emission by biexcitonic molecules.[31,32] Here, we show that this exciton-mediated

4

gain regime persist at pair densities well above the expected Mott density, where a transition of the exciton/molecule gas into an electron-hole plasma is expected. At ~ 20000 cm^{-1}, the saturated material gain in this regime is significantly larger than for comparable zero-dimensional materials, such as state-of-the-art CdSe/CdS or perovskite nanocrystals, and explains the observations of large modal gains in literature.[25,33–35] Apart from the exciton-mediated regime, a charge carrier cooling bottleneck manifests itself, which results in the peculiar co-existence of neutral excitonic species with unbound, hot electrons and holes. This combination leads to large, up to 10^5 cm^{-1}, and broadband material gain and luminescence, a second regime. At the same high excitation densities, we inferred a remarkable preservation of the exciton polarizability, as evidenced by optical pump-terahertz probe experiments, and heavy and light-hole exciton oscillator strength, both of which indicates that a pure Mott-type transition does not occur. Our results show that even though strong excitonic features are not beneficial for the development of truly broadband gain, they do significantly increase the achievable material gain magnitude. Moreover, the extreme stability of the exciton gas in colloidal 2D materials will be beneficial for applications relying on the scattering of excitons at high density, such as exciton-polariton lasers.[36]

2 Experimental Procedures

Synthesis of 4.5 ML platelets   Synthesis of 4.5 monolayer CdSe nanoplatelets was carried out by degassing cadmium myristate (0.34 g), Se (24 mg) and ODE (25 mL) in a three necked flask in vacuum and backfilling with N$_2$.[7,20] To this solution, 0.08 g of cadmium acetate was added at 205 °C when the solution turned yellow. Next, the solution was heated at 240 °C for 10 minute and 1.6 g of cadmium oleate in ODE was added at end. Samples were washed with a hexane/ethanol mixture. For spectroscopy, the CdSe platelets were dispersed in a transparent solvent (hexane) to achieve optical densities of 0.1 at the first heavy-hole exciton transition (510 nm). The photoluminescence quantum yield was determined using

an integrating sphere after CW photo-excitation at 400 nm.

Quantification of absorbed photons per platelet The average number of absorbed photons (or photo-generated electron-hole pairs) at time zero, here labeled $\langle N \rangle$, generated by a pump pulse at wavelength λ was calculated as:

$$\langle N \rangle = J_{ph} \times \sigma_a \tag{1}$$

Here J_{ph} is the photon fluence in photons/cm^2, σ_a is the absorption cross section of the platelets and A_λ is the sample absorbance at the pump wavelength. The beam size used for calculating J_{ph} is measured using a Thorlabs CCD Camera Beam profiler. The additional factor corrects for variation of the pump fluence along the pump beam path length. The cross section is determined starting from the intrinsic absorption coefficient (see Supporting Information 2).

Ultrafast transient absorption spectroscopy Samples were pumped using 110 femtosecond pulses (1 kHz) at varying wavelengths, created from the 800 nm fundamental (Spitfire Ace, Spectraphysics) through non-linear frequency mixing in an OPA (TOPAS, Light Conversion). Broadband probe pulses were generated in a CaF$_2$ crystal using the 800 nm fundamental. The probe pulses were delayed using a delay stage with maximum delay of 3.3 ns (Newport TAS). Noise levels of 0.1 mOD (RMS) are achieved by averaging out over 5000 shots. The probe spectrum covers the VIS-NIR window from 350 nm up to 700 nm. Using 2 mm path length cuvettes, the samples were stirred during pump-probe measurements to avoid effects of photo-charging and sample degradation. Only at extreme densities ($\langle N \rangle > 150$) was sample degradation observed. No air-free sample handling was required as CdSe platelets are, under our conditions, insensitive to oxidation as is evidenced by a lack of PL peak shift or change in photoluminescence quantum yield when exposing samples to ambient conditions.

Ultrafast Photoluminescence Spectroscopy For (ultrafast) photoluminescence (PL) spectroscopy, samples were measured using a cuvette with a 1 mm optical path length and an optical density of 0.1 at the heavy-hole absorption peak to avoid strong re-absorption. The quantum yield was determined using an integrating sphere with exitation at 400 nm. For the ultrafast experiments, samples were translated along 1 axis to avoid photo-charging. The detection of the broadband PL on femtosecond timescales was made possible by using a newly developed transient grating technique by Chen *et al.*.[37] A Ti:Sapphire amplifier system (Spectra-Physics Spitfire Ace) operating at 3 kHz generating 100 fs pulses was split into two parts. One part was frequency doubled using a BBO crystal and focused to a 70 μm spot on the sample. The photoluminescence is collimated using an off-axis parabolic mirror and refocused on a polished slice of fused silica. The second part of the 800 nm output was split using a 50:50 beam splitter creating two gate beams that are focused on the fused silica with a crossing angle of 5 degrees. The instantaneous grating generated by the interfering gate beams create an instantaneous gate which is used to temporally resolve the decay over a broad wavelength range. The scatter of the pump beam was suppressed using a 430 nm long-pass filter and the pump was set a magic angle relative to the PL collection. Data is averaged over 15000 shots for every time delay.

Terahertz spectroscopy Samples were photo-excited by optical pump pulses of wavelength 480 nm and the photoconductivity due to mobile charge carriers and the polarizability of excitons was probed by single cycle THz pulses. The real part of the THz conductivity is due to in-phase charge velocity in the probing THz field and leads to a reduction of the amplitude of the THz field.[38,39] The imaginary THz conductivity is due to the out-of-phase velocity of charges and the polarizability of excitons, leading to a phase retardation of the THz field.[39–43] Single cycle terahertz pulses were generated in a ZnTe non-linear crystal by optical rectification of 800 nm optical pulses of duration 45 fs, delivered from a chirped pulse amplified femtosecond laser system (Mira, Coherent), with a frequency of 1.4 kHz.

The generated THz pulses were detected in a ZnTe crystal by the electro-optic effect with a chirped optical detection pulse, which encodes and decodes the entire THz pulse in a single laser shot. Optical pulses of wavelength 480 nm were generated in an optical parametric amplifier (TOPAS, Coherent). The THz conductivity due to charge carriers and excitons at time t after the laser pump pulse, that generates charges and excitons, was obtained from the differential THz field given by $\Delta E(t_p, t) = E_{excited}(t_p, t) - E_{unexcited}(t_p)$ with $E_{excited}(t_p, t)$ and $E_{unexcited}(t_p)$ the transmitted THz field in the presence and absence of optical pumping, respectively. t_p is the delay between the THz generation and detection pulse. The real THz conductivity was obtained from the ratio $\frac{\Delta E(t_p^{max}, t)}{E_0(t_p^{max})}$, where t_p^{max} is the time at which the amplitude of the THz field is maximum, according to:[44–46]

$$\Delta\sigma_R(t) = \frac{2n_{sol}c\epsilon_0}{L} \frac{\Delta E(t_p^{max}, t)}{E_0(t_p^{max})} \tag{2}$$

with the refractive index of the solution obtained from the Maxwell Garnet model,[47] c the speed of light in vacuum, ϵ the permittivity of free space, L the sample thickness. The imaginary THz conductivity was obtained from the differential THz field with t_p^{zero} the time at which the THz field is zero, according to:[41,42,45]

$$\Delta\sigma_I(t) = \frac{2n_{sol}c\epsilon_0}{L} \frac{\Delta E(t_p^{zero}, t)}{E_0(t_p^{max})} \tag{3}$$

Material Overview CdSe platelets with a thickness of 1.37 nm, *i.e.* 4.5 monolayers, were synthesized according to Ihturria *et al.*[7,20] and their lateral dimensions were determined using brightfield transmission electron microscopy (TEM). While the measurements were repeated on multiple samples, all the data shown in the manuscript were recorded on a sample measuring 34×10 nm^2, see Figure 1a and Supporting Information S1. These dimensions are well above the ~ 2 nm Bohr diameter of the exciton, see further, leading to overall weak in-plane 2D confinement. Figure 1a shows the intrinsic absorption and spontaneous emission spectrum of a dispersion of CdSe platelets in n-hexane. As is common for direct gap II-VI
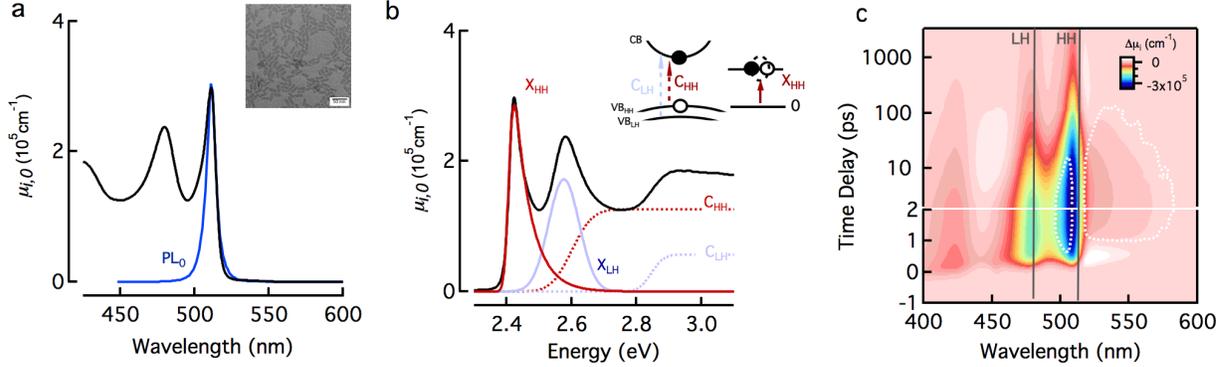
Figure 1: 4.5 monolayer (ML) colloidal CdSe quantum wells (a) Photoluminescence (blue) and linear absorption spectrum (black) of the CdSe nanoplatelets dispersed in n-hexane, where the latter is normalized to represent the intrinsic absorption coefficient $\mu_{i,0}$.[48] Inset: Transmission Electron Microscope (TEM) image showing an average lateral area of 34×10 nm^2 and no signs of stacking. (b) Absorption spectrum versus photon energy, decomposed into free carrier (C, dashed) and exciton (X, solid) contributions, both originating from the heavy (HH, red) and light hole (LH, blue) valence bands. Inset depicts the free carrier and exciton transitions. (c) Map of $\Delta\mu_i$, in cm^{-1}, for 400 nm photo-excitation creating $\langle N \rangle = 84$ as function of time (vertical axis) and probe wavelength (horizontal axis). The grey vertical lines indicate the position of the heavy (HH) and light (LH) exciton resonances. The white dashed contour indicates the regions where $|\Delta\mu_i| > \mu_{i,0}$, *i.e.* where net optical gain occurs.

semiconductor quantum wells, two excitonic features are observed, attributed to the heavy (HH, 510 nm) and light hole (LH, 480 nm) exciton transitions.[7,49] The spontaneous photoluminescence (PL) has a high quantum yield of $> 50\%$ (see Methods) and shows no Stokes shift, indicating the absence of strong phonon-coupling,[50] fine-structure relaxation,[51] or spurious effects such as charging, exciton localization or trap-emission.[49] We represent the absorbance spectrum as an intrinsic absorption coefficient $\mu_{i,0}(\text{cm}^{-1})$, a quantity that is independent of the concentration of platelets in the dispersion analyzed. $\mu_{i,0}$ can be calculated through theory as $\mu_{i,0}(300) = 5.9 \times 10^5$ cm^{-1}, see Supporting Information S2, as validated experimentally by Achtstein *et al.*[30] Besides providing a means of normalizing linear and transient spectra, $\mu_{i,0}$ enables us to calculate the absorption cross section σ of a single platelet from the relation $\sigma(\lambda) = \mu_{i,0}(\lambda) \times V$, with V the platelet volume.[48] This brings us to a cross section of 8×10^{-14} cm^2 at 400 nm for the platelets used here. Following the well-established

9

methodology of epitaxially grown quantum wells, Figure 1b shows a decomposition of the absorbance spectrum into (C) step-like features representing 2D-continuum transitions and (X) narrow resonances representing the excitonic transitions.[22,49] This decomposition shows that the sharp exciton features are actually superimposed on a broadened step-profile, typical for the 2D density of states, which is due to free carrier transitions between the first of the 2D heavy-hole states to the first 2D conduction-band states C_{HH}, see also Inset of Figure 2b. At higher energy, a similar step associated with the light hole valence band is observed, denoted as C_{LH}. The fit also enables us to estimate the exciton binding energies $E_{b,X}$ as 193 $\pm$5 meV (HH exciton) and 277 $\pm$13 meV (LH exciton). Such figures are in excellent agreement with literature,[52,53] where the large values for the exciton binding energies are confidently ascribed to the reduced screening of the Coulomb interaction compared to bulk, given the low permittivity environment consisting of ligands and solvent.[15,50] Using the exciton binding energy, we can calculate the Bohr radius of the 2D HH exciton using $m_r = 0.085$, $a_{B,HH} = \frac{\hbar}{\sqrt{2m_r E_{b,2D}}} = 1.52$ nm.[54] Given the area S of the nanoplatelets, we can define $\langle N_f \rangle = (\pi a_{b,HH}^2)^{-1} \times S$ as the number of excitons required to physically occupy all of the nanoplatelets surface area, *i.e.* the average inter-exciton distance is the Bohr diameter. For our sample, this amounts to 45 excitations per platelet, a number that sets a scale for $\langle N \rangle$ in this particular system.

3   Results

We analyzed the development of optical gain in dispersed CdSe platelets by a combination of femtosecond pump-probe transient absorption (TA), ultrafast photoluminescence (PL) spectroscopy and optical pump - terahertz probe spectroscopy (OPTP); see Methods section for technical details. All techniques involve the excitation of an ensemble of dispersed platelets using a 110 fs laser pulse at 400 nm, unless mentioned otherwise. In TA, photo-excitation is followed by probing the change in absorbance $\Delta A(\lambda, t) = A(\lambda, t) - A_0(\lambda)$, where A is the

absorbance after photo-excitation and A_0 the absorbance in absence of pump pulse – as a function of wavelength and pump-probe time delay. Note that the occurrence of optical gain, or net stimulated emission, at a given wavelength is most clearly evidenced by a negative non-linear absorbance $A = \Delta A + A_0 < 0$.

Starting from this non-linear absorbance $A(\lambda, t)$, the time-and wavelength dependent intrinsic absorption coefficient of the NC under study can be calculated as:

$$\mu_i(\lambda, t) = A(\lambda, t)/A_0(300)\mu_{i,0}(300) \tag{4}$$

see also Supporting Information S2.[30] When μ_i turns negative, we have net stimulated emission for which $-\mu_i = g_i$ can be identified as the material gain. This quantity is independent of the measurement conditions and can be translated to any device or thin-film context through a rescaling with the appropriate modal confinement and volume fraction.[33]

Figure 1c shows a 2D time-wavelength map of $\Delta \mu_i$ recorded on a dispersion of nanoplatelets using excitation at 400 nm. As outlined in the Methods section and Supporting Information S2, the average excitation number $\langle N \rangle$ such a fluence brings about per platelet can be calculated from the product $J_{ph} \times \sigma$ of the photon flux and the absorption cross section, an exercise yielding $\langle N \rangle = 84$ for the data represented in Figure 1c. At these pumping levels, pronounced, long lived bleach features arise at the HH and LH exciton positions due to state-filling. Importantly, the absorbance at the pump wavelength remains nearly unaffected, implying no corrections are needed for the absorbed number of photons. At early times, a short-lived photo-induced feature occurs near 530 nm. This photo-induced absorption gets overtaken by a bleach signal at later times and was assigned to exciton-molecule transitions, opposed to the common notion of spectral shifts.[31] Comparing the $\Delta \mu_i$ signal to $\mu_{i,0}$, we can readily identify regions of the 2D map where net optical gain occurs. These are indicated by the white dashed contour line in Figure 1c and remarkably show up both at the low and high energy side of the HH resonance.

In order to evaluate optical gain more precisely, we map out the regions of the spectrum where the material gain $g_i = -\mu_i$ turns positive. Figure 2a shows such a false color map for a higher excitation density corresponding again to an average photo-excitation density of $\langle N \rangle = 84$. We observe two distinct regimes of optical gain, separated from each other by the persisting heavy-hole absorption at 510 nm. First, an $\approx$ 60 nm (250 meV) wide gain band red-shifted from the HH-exciton peak is observed which persists for *ca.* 100 ps. This gain window coincides perfectly with reports on amplified spontaneous emission and lasing experiments on 4.5 ML CdSe nanoplatelets and recent theoretical work, see also Supporting Information S3.[22,31] At these high pump powers, an unexpected second window of optical gain develops at the high energy side of the HH-resonance. It offers significantly larger gain than the low energy band, builds up instantaneously, but is only sustained until $\approx$10 ps after photo-excitation. Figure 2b shows the map of the PL under similar conditions of optical pumping as in Figure 2a. The emission spectrum is clearly broadened towards lower and higher photon energy compared to the spontaneous emission of a single exciton. Note that the spectrum decays asymmetrically, showing a shorter $\approx$ 10 ps lifetime for the high energy luminescence and a longer $\approx$ 100 ps lifetime for the red-shifted luminescence, overall very comparable to the material gain dynamics shown in Figure 2a.

3.1   Gain Bands

To deepen our understanding of both gain regimes, we sweep the photo-generated density – or average number of excitations per platelet $\langle N \rangle$ – over two orders of magnitude, from nearly single excitations to close to 112 charge pairs per platelet. Note that the highest flux corresponds to a 2D pair density of 3.4×10^{13} cm^2. Figure 2c shows the intrinsic absorbance μ_i at 2.5 ps for these increasing densities. We observe that gain initially builds up on the low energy (long wavelength) side of the HH resonance. This first gain window is sustained throughout the entire density range. The gain in the blue-shifted regime is observed only when the excitation exceeds *ca.* 40. A number of intriguing observations can already be

12

made at this point: the gain at the high energy side is disruptively larger than the low-energy gain; both the heavy and light hole exciton absorption persists, showing only slight saturation and effectively counteract broadband gain development; and at high density, a reduction of the absorbance plateau at shorter wavelengths (¡480 nm) is observed.

Zooming in on the net material gain $g_i = -\mu_i$ in Figure 2d, shows that for the low energy gain band, the intrinsic gain coefficient in cm^{-1} reaches up to 18000 cm^{-1} and eventually saturates close to 84 excitations per platelet. Quantitative variable stripe length experiments verify such large gain coefficients are indeed achievable, see Supporting Information S3, and line up with the report of Guzelturk *et al.*[25]

The gain at the blue side shows no signs of saturation and is also disruptively larger with values close to $10^5 cm^{-1}$. A more detailed analysis of the gain threshold is shown in Figure 2e, see also Supporting Information S4, where we observe that the low energy gain band has a threshold of 4.1 ± 0.5 and the high energy gain band of 35 ± 2, see also Supporting Information S4.

Finally, Figure 2f shows a similar fluence dependence as Figures 2c-d for the PL after 2.5 ps. Also here, a transition occurs at *ca.* $\langle N \rangle = 35$ which is perhaps more clearly observed looking at the wavelengths (energies) for which the luminescence has its half-maximum value, as is shown in the inset of Figure 2f. A gradual increase at the low energy side clearly contrasts the disruptive jump on the high energy side near $\langle N \rangle = 35$. These results show that not only are nanoplatelets able to amplify incoming probe light in the high energy gain window, they also exhibit spontaneous emission in the same spectral region, with a similar density-dependent onset. This is crucial for their use in lasers since the material's ability to amplify its own spontaneous emission is what sets it apart from optical amplifiers.

As shown elsewhere, we assign the low energy gain band to stimulated emission from excitonic molecules.[31] Such a biexcitonic molecule is a bound two-exciton state with a binding energy $E_{b,M} \approx 45$ meV for 4.5 ML CdSe platelets, outlasting thermal energy at room temperature and typical optical phonon energies of CdSe.[22,31,49] This complex can recombine
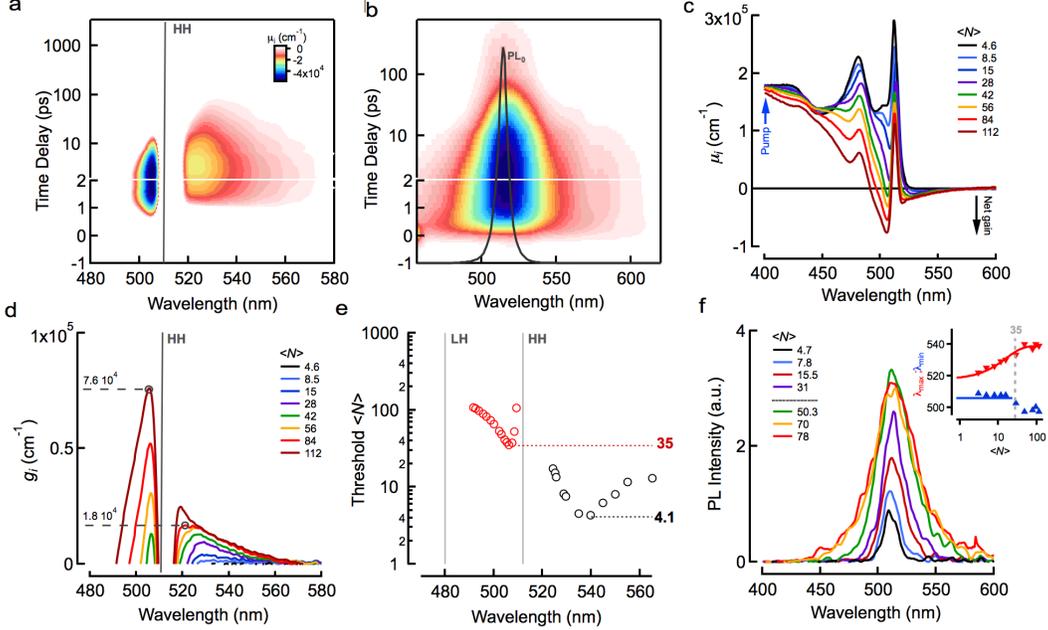
Figure 2: Optical gain at high carrier density after excitation with 400 nm. (a) 2D time-wavelength map of the intrinsic absorption coefficient μ_i (cm^{-1}) for $\langle N \rangle = 84$ where we limit the colour scale to negative values showing net gain: $g_i = -\mu_i > 0$. The vertical line indicate the position of the heavy-hole exciton resonance. (b) 2D time-wavelength map of the PL taken at the same excitation density as (a). Black trace is the spontaneous emission for $\langle N \rangle \ll 1$. (c) Intrinsic absorption coefficients taken 2.5 ps after photo-excitation with a 400 nm pump pulse for densities ranging from 4.6 to 112 excitations per platelet. (d) Material gain spectra g_i for the same carrier densities as (c). (e) Required $\langle N \rangle$ to achieve transparency, $\mu_i(2.5\text{ps}) = 0$, as function of wavelength. Optical gain is achieved at 4.1 and 35 in the red and blue-shifted gain regimes respectively. (f) PL at 2.5 ps for increasing pair density from 4.7 to 78. The inset shows the FWHM wavelengths of the PL spectra.

radiatively to a single exciton state, giving rise to stimulated emission and net amplification in a narrow band on the low energy side of the heavy-hole exciton absorption. The quantified material gain coefficients of the excitonic molecule gain mechanism shown here are close to 1 order of magnitude larger than observed for state-of-the-art CdSe/CdS or perovskite quantum dots,[33–35] which rationalizes recent reports on extremely small footprint lasers operating under low excitation power.[22–24] Supporting Information S5 shows that across the entire density range, exciton-exciton annihilation is the main culprit for the vanishing carrier density and hence the overall optical gain lifetime of *ca.* 100 ps, as confirmed by other reports.[55–57]

14

The exciton-mediated red-shifted gain window observed at low density persists through the entire density range and shows a saturation close to 100 excitations, see Figure 2d. The latter already indicates that excitonic species can indeed persist up to such high carrier densities. In particular for the biexcitonic molecules, which show a much smaller stabilization energy compared to excitons, this result is remarkable. An initial confirmation is found in the absence of a full collapse of the exciton oscillator strength as is observed *via* the preservation of the exciton luminescence, gain and absorption features, see Figure 2. However, before we analyze the limited exciton saturation in more detail, we want to unambiguously confirm the existence of excitons at high density.[58]

3.2   Excitonic Stability at High Density

To this end, we employ optical pump-THz probe spectroscopy as, similar to previous studies on 2D InSe nanosheets,[59] one can use these measurements to characterize the nature of photo-excited species. The real component of the THz conductivity is due to free mobile charges moving with velocity in-phase with the THz field, while the imaginary conductivity is due to the out-of-phase velocity of charges (resulting from scattering) and the polarizability of excitonic species (see Methods).[39,40]

Figure 3a shows the THz conductivity as a function of time after photo-excitation for $\langle N \rangle = 6$ and 53. The real conductivity is much smaller than the imaginary component for both densities, which is a strong qualitative indication for a significant contribution from excitons. To get more insight into the contribution of excitons we plot the kinetics of the optical bleach at the HH transition due to excitons on top of the imaginary THz conductivity for comparable excitation densities. The decay kinetics of the bleach and imaginary THz conductivity are similar at lower and higher densities, indicating that the imaginary THz conductivity is mainly due to excitons.

The initial real THz conductivity $\Delta \sigma_R$ is given by:[44,59]

$$\Delta\sigma_R = \frac{eN_a\phi(n)\sum\mu_R}{L} \quad (5)$$

with $\sum\mu_R$ the sum of the real components of the electron and hole mobility, ϕ the quantum yield of charges, e the elementary charge and N_a the number of absorbed photons per unit area in the sample solution with cuvette length L. As denoted, ϕ depends on the average pair density $n = \langle N\rangle/S$ where S is the average platelet area. The imaginary THz conductivity $\Delta\sigma_I$ is given by the sum of the contribution of (localized) charges and excitons, according to:[44,45,59]

$$\Delta\sigma_I = \frac{eN_a}{L} \times [\sum\mu_I\phi(n) + \frac{\alpha\omega}{e}(1 - \phi(n))] \quad (6)$$

with $\sum\mu_I$ the sum of the imaginary electron and hole mobility, α the polarizability of excitons and ω the radian frequency of the THz electric field. The imaginary THz conductivity in Figure 3b increases close to linearly with $\langle N\rangle$ (or n). The sub-linear increase of the contribution of free charges observed in the real conductivity indicates $\phi(n)$ increases strongly sub-linearly. Given equation 2 and the observed linear increase with n, this implies a significant contribution of the second term in Equation 2, *i.e.* of excitons.

The fraction ϕ of free charges is dictated by the Saha equilibirium $e + h \rightleftharpoons X$, which assumes a thermal equilibrium between excitons and free charge carriers. In Supporting Information S6, this equilibrium is worked out formally. Using the Saha model at a temperature of 293 K, and fitting that to the experimental data with $\sum\mu_{I,R}$ and the exciton polarizability α as adjustable parameters, yields the drawn curves in Figures 3b. The real conductivity is reproduced with $\sum\mu_R = 54 \pm 12$ cm^2/Vs. For the imaginary conductivity we found $\sum\mu_I = 7 \pm 5$ cm^2/Vs and $\alpha = 3.1 \pm 0.2 \times 10^{-36}$Cm^2/V. The imaginary charge mobility and the exciton polarizability for the 4.5 monolayer CdSe platelets studied in the current work, are close to those reported earlier for similar CdSe platelets.[47,53]

We remark that the Saha equation can fit the data reasonably well beyond the broadband

gain onset of $\langle N \rangle = 35$, see Figure 3b. We should however proceed with caution in this regime for two reasons. The temperature of the system is not well defined beyond this density and most likely above room temperature, as is evidenced by detailed analysis of the PL (see further), and (b) full occupation of the platelet occurs around the same number, $\langle N \rangle_f = 45$, as derived earlier. The first observation complicates the validity of the Saha fitting procedure as thermal equilibrium is not guaranteed, whereas the second observation indicates possibly stronger carrier scattering limiting the mobility and hence possibly saturating the transient real conductivity.

In any case, the THz results unambiguously show that across the entire density range probed in this work, excitons are present with no significant change in the polarizability compared to the isolated, low density regime. This agrees with the observation that the redshifted gain window, assigned to excitonic species, can persist up to the highest densities used here. For the highest carrier density employed in this work (112), the average inter-exciton distance is only $d_s = 2\sqrt{\frac{S}{\pi \times \langle N \rangle}} = 1.9$ nm, fairly close to the Bohr radius estimated earlier. Though exciton-carrier phase diagrams can be very complex, a general understanding is that a so-called Mott-type transition should occur at these separations. Closely tied to the transition of an exciton gas into a conductive phase is the saturation and spectral shifting of the exciton absorption line itself. It is well known that the oscillator strength of the exciton transitions can diminish and vanish due to state-filling and screening-induced renormalization effects.[10] In concert with this, the exciton line will also undergo spectral shifts for increasing density due to a balance between renormalization of the band gap (redshift) and reduction in exciton binding energy (blueshift).[60–62] Figure 3c shows the evolution of the normalized oscillator strength of the HH -exciton line, extracted from the integrated HH-peak area (see Supporting Information S2), and the heavy-hole spectral shift ΔE_{HH}, for increasing excitation density. A qualitative fit, $\frac{f}{f_0} = \frac{1}{1 + \frac{\langle N \rangle}{\langle N \rangle_s}}$, to the oscillator strength indicates a characteristic saturation density $\langle N \rangle_s = 12.7$. A full Mott-transition is however not observed as the oscillator strength persists up to $\langle N \rangle = 112 \approx 10 \langle N_s \rangle$, with a lingering strength of

ca. $0.25f_0$. This observation indicates new types of carriers, or interactions between them, manifest themselves at higher density, a point we will elaborate further in the following section.

Finally, the exciton line shows a clear red-shift indicating that band gap renormalization overtakes the blueshift that would originate from a binding energy reduction through increased screening of the exciton.[14] Our quantitative observations on CdSe are in-line with recent observations on other high binding energy 2D materials such as WS_2, where similarly a red-shift and no full saturation of the exciton line was observed until densities of 5×10^{12} cm^{-2}, equivalent to $\langle N \rangle = 16$ for our experiments, yet at slightly higher densities, Chernikov *et al.* showed the exciton line does get fully saturated and a transition to free carrier-mediated gain takes over.[18,60]
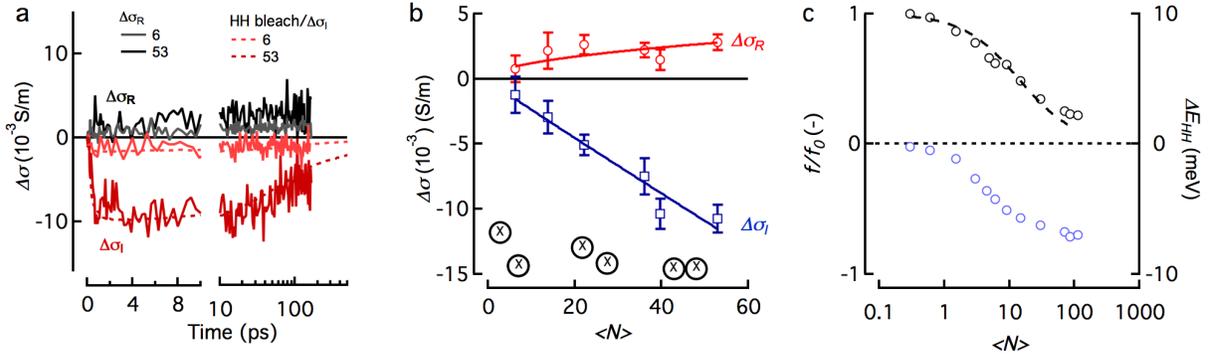
Figure 3: THz spectroscopy (a) Real (positive traces) and imaginary (negative traces) components of the THz conductivity as a function of time after photo-excitation with $\langle N \rangle$ equal to 6 and 53. The optical bleach at the heavy hole (HH) exciton transition at comparable densities is shown for comparison with the imaginary THz conductivity. (b) Measured real (red circles) and imaginary (blue squares) THz conductivity averaged between 6 and 10 ps after photo-excitation as a function of $\langle N \rangle$, together with fitted results from the Saha model (solid lines). Inset below shows a schematic depiction of the inter-exciton distance for this density range. (c) Reduction of normalized HH oscillator strength (red circles) and HH spectral shift ΔE (blue triangles), normalized to the HH binding energy, for increasing carrier density.

3.3   Gain *via* Unbound Charge Carriers

Having established the excitonic nature of the universal gain regime at low photon energy, it remains an open question what causes the short-lived broadband gain and luminescence at high photon energy just after strong photo-excitation. To deepen our understanding, we first conceptualize how charge carrier thermalize and excitons are formed in direct gap polar semiconductors. Upon photo-excitation with 400 nm (3.1 eV), free electrons and holes with significant excess energy are created. These 'hot' carriers have to cool down by optical phonon emission and finally condense into a heavy-hole exciton, see Figure 4a.[49,63] This is quite a remarkable process as the stabilization of the exciton alone, *i.e.* its binding energy, requires the dissipation of close to 200 meV. Given typical phonon energies of $E_{LO,CdSe} \approx 26$ meV, this implies multiple optical phonons need to be emitted.[50] Several reports in literature indicated that this coupling to phonons is relatively weak for single excitons and gets even more slowed down with increasing excitation density, hence slowing down exciton formation after non-resonant excitation.[50,64,65] Nonetheless, we observe a sub-picosecond, near resolution-limited, buildup of the band edge exciton population and the associated gain at low exciton densities.

To understand how a cooling bottleneck can still manifest with such fast single exciton formation, we should consider the accumulative nature of the phonon emission process, see also Figure 4a.[49,63] At early times, carriers cool down extremely fast to the band edge by rapid phonon emission, denoted as stage (1) in Figure 4a, giving rise to fast buildup of exciton PL and band-edge bleach, stage (2). However, as more carriers cool down the phonon population increases up to a point where the temperature (occupation) of (a subset of) the phonon mode(s), generalized as T_q, exceeds that of the electronic system, generalized as T_e. At this point, net energy transfer to the phonon bath will substantially reduce, giving rise to a cooling bottleneck for the remaining carriers. Overall, this would result in the formation of a hot electron-hole gas which cannot cool down effectively to form excitons. This will eventually lead to spontaneous and also stimulated emission from unbound charge carriers from higher energy free carrier states.
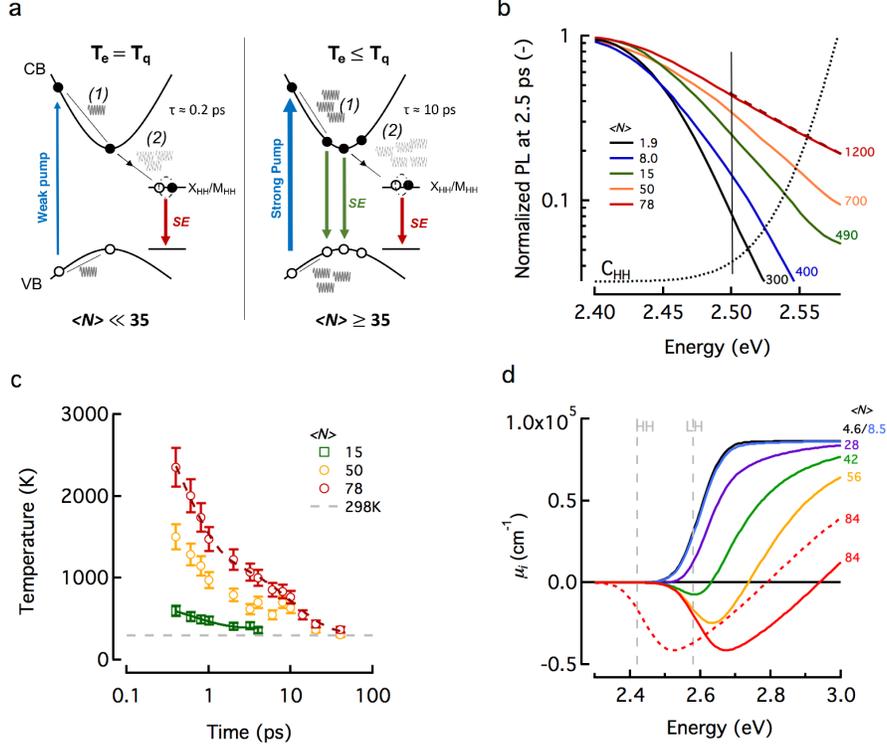
Figure 4: (a) Schematic explaining the effect of a phonon emission bottleneck on the various stages (1),(2) of exciton formation in a low (left) and high (right) density regime and the associated stimulated emission (SE) pathways. (b) Normalized photoluminescence (PL) for increasing pump fluence, 2.5 ps after photo-excitation with 400 nm (3.1 eV). The dashed fits indicates a Boltzmann approximation to the decaying high energy tail of the PL, the latter delineated by the vertical solid line. The thus extracted temperatures are labeled on the traces from 300 K (black) to 1200 K (red). Dotted black line is the free charge carrier transition C_{HH}, see also Figure 1b. (c) Dynamics of carrier temperature for various excitation densities. Solid lines are restricted fits, see main text. (d) Calculated intrinsic absorption coefficient of the heavy-hole associated free carrier transition for increased carrier density. The dashed red line shows the result at the highest density combined with a band gap renormalization (BGR) of 150 meV.

Key elements to validate the proposed model are (a) the (prolonged) occupation of high energy levels corresponding to unbound charges and (b) an increase of the overall carrier temperature, *i.e.* a modified distribution of charge carriers over those high energy states. The TA and luminescence data in Figure 2c,f already show that we can indeed attain a significant amount of carriers occupying energy levels blue-shifted from the HH line since we achieve spontaneous emission and net amplification of incoming probe light in that spectral

window. As the TA data is congested due to the overlap of several spectral features (bleach, induced absorption, shifts, ..), we focus here on the PL data to extract additional information on the unbound charge carrier distribution, *i.e.* their temperature and absolute number density.

Figure 4b shows the high energy tail of the normalized photoluminescence (PL) spectrum 2.5 ps after photo-excitation with 400 nm, for increasing excitation density from $\langle N \rangle = 1.9 - 78$. We clearly observe both an increased emission at higher energy and a change in the slope of the high energy tail. The latter indicates that the distribution of the carriers over the high energy levels is changing, not just the occupation of the levels themselves. Fitting the decaying tail with a Boltzmann distribution,[49] $I(\hbar\omega) \propto e^{-\frac{E - E_f}{k_B T_e}}$, we are able to extract an effective carrier temperature T_e which starts off at 300 K for low excitation density and reaches up to 1200 K for $\langle N \rangle$ close to 80. A Boltzmann fit is a good approximation if we restrain the fit to high energies (> 2.5 eV; 496 nm) effectively matching the expected energy range of free carrier related transitions, shown by the dotted black curve in Figure 4b. Supporting Information S7 shows moreover that quasi-Fermi level shifts are limited.[49] The lower density limit corresponds well to the data of Sippel *et al.*, who found similar carrier temperatures at low densities.[64]

Figure 4b shows the full dynamics of the extracted temperature for three initial excitation densities: 15, 50 and 78. A single component fit of the lowest density trace shows that the temperature decay is initially very fast with a characteristic lifetime of $\tau_1 = 355 \pm 35$ fs. Fixing this fast lifetime, we can also do a restricted two-component fit on the high density kinetic trace and find a second component of 10 ± 1.4 ps. The latter matches well with the observed gain lifetime in the high energy region, see Figure 2a. This two-stage cooling corresponds well to the notion of initial fast LO phonon emission followed by a bottleneck caused by overheating of the phonon bath.

Having established that there is a population of high energy unbound carriers with elevated temperature, we can now rationalize their role in optical gain development. Looking

21

closer at the TA data of Figure 2c, we observe that at high enough density (Figure 2c), the high-energy plateau ($<$ 495 nm; 2.50 eV) of the absorbance starts to collapse. Looking back at Figure 1b, this plateau is formed by the staircase absorption profile of a 2D electron gas, in particular from the quantized heavy-hole valence band to the conduction band. Filling up these energy levels will indeed lead to a bleach of the plateau C_{HH} and eventually optical gain, as is observed for densities above *ca.* 35 electron-hole pairs. To gain more insight, we calculated the intrinsic absorption coefficient for varying carrier densities, considering only the heavy hole continuum C_{HH} of Figure 1c, see also Supporting Information S7. In Figure 4d, we obtain both the experimentally observed collapse of the absorbance and a clear transition from net absorption to optical gain. A detailed zoom around the gain threshold is shown in Supplementary Figure S6 and reveals a gain threshold close to 20 excitations. This number is substantially larger than the molecule mediated gain threshold (4.1) but slightly lower than the observed $\langle N \rangle = 35$, see Figure 2e. This is to be expected since not all excitations are unbound charge carriers and competing LH/HH absorption will counteract the gain buildup. The correspondence of the experimental high energy gain data with the classical quantum well gain model is excellent as also the gain magnitude, *e.g.* 5×10^4cm^{-1} for $\langle N \rangle = 84$ is retrieved. However, the gain from free carriers is at slightly higher energy than observed experimentally. It is however well established that strongly photo-excited (2D) semiconductors show strong band gap renormalization (BGR).[61] Estimates based on universal models indicate shifts of 2 excitonic Rydbergs (Ry$_{2D}$ = $\frac{2e^2}{\epsilon_0 a_{B,2D}}$) up to a density of $\langle N_f \rangle$(=45) and reaching even up to 4 Ry$_{2D}$ for higher densities. For CdSe, this would amount to shifts of 60 meV at low density and up to 240 meV at higher density. Figure 4c shows that such a moderate 150 meV renormalization for the highest density indeed pushes the optical gain window in between the two exciton resonances, exactly where optical gain is observed.

4 Discussion

The increased formation of free charge carriers at elevated carrier temperatures and densities over excitons explains the observations made in Figure 3c on the lack of exciton saturation and blueshift. Indeed, exciton saturation through state-filling will be ineffective since carriers do not thermalize to occupy the band edge levels and additionally, a gas of unbound two-dimensional charge carriers is considered less effective at screening Coulomb interactions than cold excitons.[14] Also the persistent exciton redshift, as was observed in Figure 3c, can be rationalized this way since the position of the exciton transition is a balance between band-grap renormalization (BGR) and screening-induced blueshifts. The latter are too weak to overcome the substantial BGR and the overall line redshifts. The remarkable absence of a full Mott-type transition merits further theoretical investigation. Several estimates of this Mott density exist, based on dynamic or static screening arguments.[66] Static screening would put the Mott transition at $na_B^2 = 0.1$, which for our system would amount to a mere $\langle N \rangle \approx 14$, clearly a huge underestimation.[14]

A possibe explanation for the high energy gain window could be the emission/gain from multi-excitons, similar to what is observed in colloidal 0D CdSe-based quantum dots.[32,34] It is however important to stress that the photo-physics of excitons in 2D materials is fundamentally different of that found in zero-dimensional systems. The example of biexciton formation is illustrative for this purpose.[31] Whereas in a 0D system, excitons have due to spatial localization no choice than to form the bi-exciton state, either repulsive or attractive, this is not valid for a 2D system with lateral extent (326 nm^2) much larger than the exciton size (7.2 nm^2). Indeed, if the interactions between excitons are repulsive in a 2D system, the excitons simply do not stabilize and retain their single exciton characteristics. As such, repulsive exciton interactions cannot explain the blue-shifted gain window. Another '0D'-argument could be that we are just observing state-fillingn where optical gain will manifest itself first on the low energy side and then span out to higher transitions, such as P-type transitions found in QDs, upon increased population.[32] First off, this contradicts

our observation that the heavy-hole exciton line persists in absorption, see Figure 2c/3c. If state-filling was applicable, it should quench similar to the absorption line in 0D quantum dots saturates (and inverts) when the population reaches (half of) the band edge degeneracy and then span out to provide gain of excited exciton states.[34] Moreover, fluorescence and gain of non-thermalized excitons holds no ground since only zero momentum (K=0) transitions are allowed for 2D excitons.[49] Finally, the density of states at the band edge is enormous in a 2D system. Even modest estimates of the number of available states N_S in the 50 meV window taken up by the HH line, puts the number at *ca.* 230, see Supporting Information S8. An additional proof that state-filling plays no role in the blue-shifted gain band is found by exciting the system at 480 nm. Significantly less energy, *ca.* 500 meV, needs to be dissipated in this case, leading to much more efficient thermalization. Using the same exciton density, we observe only limited blue-shifted gain under these conditions with a much narrower bandwidth, see Supporting Information S8, again evident that exciton state filling cannot explain the blue-shifted gain window.

5   Conclusion

We have quantified and modeled the distinctive mechanisms leading to room temperature optical gain in 2D CdSe nanoplatelets, a model system for collodial 2D materials. At high charge carrier density, a phonon bottleneck slows down hot carrier cooling leading to a unique situation of strong light amplification by unbound charge carriers, up to 10^5cm^{-1}, and excitonic molecules simultaneously. The remarkable retention of excitonic features until extreme densities indicated an absence of a full Mott-type collapse of the exciton gas, as confirmed by THz spectroscopy. Although it shows from our results that this remarkable property is not directly beneficial for development of very broadband stimulated emission due to lingering exciton absorption, it does indicate gain at high exciton densities is feasible with concomitantly high gain coefficients. Moreover, it could render other applications possible

such as high brightness LEDs or more complex devices relying on high density multi-exciton phenomena such as Bose-Einstein condensation.[67] Indeed, the latter are often hampered by exciton instability at high carrier densities, a problem which is absent in these high exciton binding energy quantum wells.[36,68] Clearly, (colloidal) 2D materials hold great promise to realize small footprint, low threshold microlasers. Hence, it would be of great interest to see how these observations translate to other 2D material systems with different types of carrier-carrier and carrier-phonon interactions such as transition metal di-chalcogenides or layered perovskites.[3,6,11]

Acknowledgement

Supporting Information Available

The Supporting Information contains information on the TEM analysis, absorption cross section and gain threshold calculation, more detailed analysis of recombination kinetics, the Saha fitting and the quantum well gain model.

References

(1) Kovalenko, M. V.; Manna, L.; Cabot, A.; Hens, Z.; Talapin, D. V.; Kagan, C. R.; Klimov, V. I.; Rogach, A. L.; Reiss, P.; Milliron, D. J. et al. Prospects of Nanoscience with Nanocrystals. *ACS Nano* **2015**, *9*, 1012–1057.

(2) Kagan, C. R.; Lifshitz, E.; Sargent, E. H.; Talapin, D. Building Devices from Colloidal Quantum Dots. *Science* **2016**, *353*.

(3) Xia, F.; Wang, H.; Xiao, D.; Dubey, M.; Ramasubramaniam, A. Two-Dimensional Material Nanophotonics. *Nat. Photon.* **2014**, *8*, 899–907.

(4) Wang, Q. H.; Kalantar-Zadeh, K.; Kis, A.; Coleman, J. N.; Strano, M. S. Electronics and Optoelectronics of Two-Dimensional Transition Metal Dichalcogenides. *Nat. Nanotech.* **2012**, *7*, 699–712.

(5) Bie, Y.-Q.; Grosso, G.; Heuck, M.; Furchi, M. M.; Cao, Y.; Zheng, J.; Bunandar, D.; Navarro-Moratalla, E.; Zhou, L.; Efetov, D. K. et al. A $MoTe_2$-based Light-Emitting Diode and Photodetector for Silicon Photonic Integrated Circuits. *Nat. Nanotech.* **2017**, *12*, 1124–1129.

(6) Manser, J. S.; Christians, A.; Kamat, P. V. Intriguing Optoelectronic Properties of Metal Halide Perovskites. *Chem. Rev.* **2016**, *116*, 12956–13008.

(7) Ithurria, S.; Tessier, M. D.; Mahler, B.; Lobo, R. P. S. M.; Dubertret, B.; Efros, A. L. Colloidal Nanoplatelets with Two-dimensional Electronic Structure. *Nat. Mater.* **2011**, *10*, 936–941.

(8) Ye, Y.; Wong, Z. J.; Lu, X.; Ni, X.; Zhu, H.; Chen, X.; Wang, Y.; Zhang, X. Monolayer Excitonic Laser. *Nat. Photon.* **2015**, *9*, 733–737.

(9) Zhao, L.; Shang, Q.; Gao, Y.; Shi, J.; Liu, Z.; Chen, J.; Mi, Y.; Yang, P.; Zhang, Z.; Du, W. et al. High Temperature Continuous-Wave Pumped Lasing from Large-Area Monolayer Semiconductors Grown by Chemical Vapor Phase Deposition. *ACS Nano* **2018**, *12*, 9390–9396.

(10) Schmitt-Rink, S.; Ell, C.; Haug, H. Many-body Effects in the Absorption, Gain, and

Luminescence Spectra of Semiconductor Quantum-well Structures. *Phys. Rev. B* **1986**, *33*, 1183–1189.

(11) Rustagi, A.; Kemper, A. F. Theoretical Phase Diagram for the Room Temperature Electron-Hole Liquid in Photo-Excited Quasi-2D Monolayer MoS_2. *Nano Lett.* **2017**, *18*, 455–459.

(12) Schmitt-Rink, S.; Ell, C. Excitons and Electron-Hole Plasma in Quasi-Two-Dimensional Systems. *J. Lumin.* **1985**, *30*, 585–596.

(13) Asano, K.; Yoshioka, T. Exciton-Mott Physics in Two-Dimensional Electron-Hole Systems: Phase Diagram and Single-Particle Spectra. *J. Phys. Soc. Jpn.* **2014**, *82*, 084702.

(14) Schmitt-Rink, S.; Chemla, D. S.; Miller, D. A. B. Theory of Transient Excitonic Optical Nonlinearities in Semiconductor Quantum-well Structures. *Phys. Rev. B* **1985**, *32*, 6601–6609.

(15) Kumagai, M.; Takagahara, T. Excitonic and Nonlinear-Optical Properties of Dielectric Quantum-Well Structures. *Phys. Rev. B* **1989**, *40*, 12359.

(16) Kozlov, V.; Kelkar, P.; Vertikov, A.; Nurmikko, A. V. Gain Spectroscopy of Excitonic molecules and its Dynamics in a ZnSe Single Quantum Well. *Phys. Rev. B* **1996**, *54*, 932–937.

(17) Ding, J.; Jeon, H.; Ishihara, T.; Hagerott, M.; Nurmikko, A. V.; Luo, H.; Samarth, N.; Furdyna, J. Excitonic Gain and Laser Emission in ZnSe-based Quantum Wells. *Phys. Rev. Lett.* **1992**, *69*, 1707–1710.

(18) Chernikov, A.; Ruppert, C.; Hill, H. M.; Rigosi, A. F.; Heinz, T. F. Population Inversion and Giant Bandgap Renormalization in Atomically thin WS_2 Layers. *Nat. Photon.* **2015**, *9*, 466–470.

(19) Zhu, B.; Chen, X.; Cui, X. Exciton Binding Energy of Monolayer WS$_2$. *Sci. Reports* **2015**, *9218*.

(20) Singh, S.; Tomar, R.; ten Brinck, S.; De Roo, J.; Geiregat, P.; Martins, J. C.; Infante, I.; Hens, Z. Colloidal CdSe Nanoplatelets, a Model for Surface Chemistry/Opto-Electronic Property Relations in Semiconductor Nanocrystals. *J. Am. Chem. Soc.* **2018**, *140*, 13292–13300.

(21) Majumdar, A.; Xu, X. Monolayer Semiconductor Nanocavity Lasers with Ultralow Thresholds. *Nature* **2015**, *520*, 69–72.

(22) Grim, J. Q.; Christodoulou, S.; Di Stasio, F.; Krahne, R.; Cingolani, R.; Manna, L.; Moreels, I. Continuous-Wave Biexciton Lasing at Room Temperature using Solution-processed Quantum Wells. *Nat. Nanotech.* **2014**, *9*, 891–895.

(23) Yang, Z.; Pelton, M.; Fedin, I.; Talapin, D. V. A Continuous-Wave Nanolaser using Colloidal Quantum Wells. *Nat. Comm.* **2017**, *8*, 143.

(24) Pelton, M. Carrier Dynamics, Optical Gain, and Lasing with Colloidal Quantum Wells. *J. Phys. Chem. C* **2018**, *122*, 10659–10674.

(25) Guzelturk, B.; Pelton, M.; Olutas, M.; Demir, H. V. Giant Modal Gain Coefficients in Colloidal II–VI Nanoplatelets. *Nano Letters* **2018**, *19*, 277–282.

(26) Gungor, K.; Demir, H. V. Highly Stable Multicrown Heterostructures of Type-II Nanoplatelets for Ultralow Threshold Optical Gain. *Chem. Mater.* **2019**, *Article ASAP - DOI:10.1021/acs.chemmater.9b00136*.

(27) Li, Q.; Xu, Z.; Mcbride, J. R.; Lian, T. Low Threshold Multiexciton Optical Gain in colloidal CdSe/CdTe Core/Crown Type-II Nanoplatelet Heterostructures. *ACS Nano* **2017**, *11*, 2545–2553.

(28) Olutas, M.; Guzelturk, B.; Kelestemur, Y.; Yeltik, A.; Delikanli, S.; Demir, H. Lateral Size-Dependent Spontaneous and Stimulated Emission Properties. *ACS Nano* **2015**, *5*, 5041–5050.

(29) She, C.; Fedin, I.; Dolzhnikov, D. S.; Demortière, A.; Schaller, R. D.; Pelton, M.; Talapin, D. V. Low-Threshold Stimulated Emission using Colloidal Quantum Wells. *Nano Lett.* **2014**, *14*, 2772–2777.

(30) Achtstein, A. W.; Antanovich, A.; Prudnikau, A.; Scott, R.; Woggon, U.; Artemyev, M. Linear Absorption in CdSe Nanoplates: Thickness and Lateral Size Dependency of the Intrinsic Absorption. *J. Phys. Chem. C* **2015**, *119*, 20156–20161.

(31) Geiregat, P.; Tomar, R.; Chen, K.; Hodgkiss, J.; Hens, Z. Room Temperature Stimulated Emission by Excitonic Molecules in Colloidal Quantum Wells. *Submitted* **2019**,

(32) Li, Q.; Lian, T. A Model for Optical gain in Colloidal Nanoplatelets. *Chem. Sci.* **2018**, *9*, 728–734.

(33) Xie, W.; Zhu, Y.; Bisschop, S.; Aubert, T.; Hens, Z.; Thourhout, D. V.; Geiregat, P. Colloidal Quantum Dots Enabling Coherent Light Sources for Integrated Silicon-Nitride Photonics. *J. Sel. Top. Quantum Electron.* **2017**, *23*.

(34) Bisschop, S.; Geiregat, P.; Aubert, T.; Hens, Z. The Impact of Core/Shell Sizes on the Optical Gain Characteristics of CdSe/CdS Quantum Dots. *ACS Nano* **2018**, *12*, 9011–9021.

(35) Geiregat, P.; Maes, J.; Chen, K.; Drijvers, E.; De Roo, J.; Hodgkiss, J. M.; Hens, Z. Using Bulk-like Nanocrystals To Probe Intrinsic Optical Gain Characteristics of Inorganic Lead Halide Perovskites. *ACS Nano* **2018**, *12*, 10178–10188.

(36) Flatten, L. C.; Christodoulou, S.; Patel, R. K.; Buccheri, A.; Coles, D. M.; Reid, B.

P. L.; Taylor, R. A.; Moreels, I.; Smith, J. M. Strong Exciton Photon Coupling with Colloidal Nanoplatelets in an Open Microcavity. *Nano Lett.* **2016**, *16*, 7137–7141.

(37) Chen, K.; Gallaher, J. K.; Barker, A. J.; Hodgkiss, J. M. Transient Grating Photoluminescence Spectroscopy: An Ultrafast Method of Gating Broadband Spectra. *J. Phys. Chem. Lett.* **2014**, *5*, 1732–1737.

(38) Hangleiter, A.; Jin, Z.; Gerhard, M.; Kalincev, D.; Langer, T.; Bremers, H.; Rossow, U.; Koch, M.; Bonn, M.; Turchinovich, D. Efficient Formation of Excitons in a Dense Electron-hole Plasma at Room Temperature. *Phys. Rev. B* **2015**, *241305*.

(39) Ulbricht, R.; Hendry, E.; Shan, J.; Heinz, T. F.; Bonn, M. Carrier Dynamics in Semiconductors Studied with Time-resolved Terahertz Spectroscopy. *Rev. Mod. Phys.* **2011**, *83*, 543–586.

(40) Lloyd-Hughes, J.; Jeon, T. I. A Review of the Terahertz Conductivity of Bulk and Nano-materials. *J. Infr. Mill. THz Wav.* **2012**, *33*, 871–925.

(41) Dakovski, G.; Lan, S.; Xia, C.; Shan, J. Terahertz Electric Polarizability of Excitons in PbSe and CdSe Quantum Dots. *J. Phys. Chem. C* **2007**, *111*, 5904–5908.

(42) Wang, F.; Shan, J.; Islam, M. a.; Herman, I. P.; Bonn, M.; Heinz, T. F. Exciton Polarizability in Semiconductor Nanocrystals. *Nat. Mater.* **2006**, *5*, 861–864.

(43) Hendry, E.; Koeberg, M.; Schins, J. M.; Nienhuys, H. K.; Sundström, V.; Siebbeles, L. D. A.; Bonn, M. Interchain Effects in the Ultrafast Photophysics of a Semiconducting Polymer: THz Time-domain Spectroscopy of Thin films and Isolated Chains in Solution. *Phys. Rev. B* **2005**, *71*, 1–10.

(44) Evers, W. H.; Schins, J. M.; Aerts, M.; Kulkarni, A.; Capiod, P.; Berthe, M.; Grandidier, B.; Delerue, C.; van der Zant, H. S. J.; van Overbeek, C. et al. High Charge

Mobility in Two-dimensional Percolative Networks of PbSe Quantum Dots Connected by Atomic Bonds. *Nat. Comm.* **2015**, *6*, 8195.

(45) Cunningham, P. D. Accessing Terahertz Complex Conductivity Dynamics in the Time-Domain. *IEEE Trans. Terahertz Sci. Technol.* **2013**, *3*, 494–498.

(46) Murphy, J. E.; Beard, M. C.; Nozik, A. J. Time-resolved Photoconductivity of PbSe Nanocrystal Arrays. *J. Phys. Chem. B* **2006**, *110*, 25455–25461.

(47) Kunneman, L. T.; Schins, J. M.; Pedetti, S.; Heuclin, H.; Grozema, F. C.; Houtepen, A. J.; Dubertret, B.; Siebbeles, L. D. A. Nature and Decay Pathways of Photoexcited States in CdSe and CdSe/CdS Nanoplatelets. *Nano Lett.* **2014**, *14*, 7039–7045.

(48) Hens, Z.; Moreels, I. Light Absorption by Colloidal Semiconductor Quantum Dots. *J. Mater. Chem.* **2012**, *22*, 10406–10415.

(49) Pelant, I.; Valenta, J. In *Luminescence Spectroscopy of Semiconductors*; Oxford University Press,, Ed.; 2012.

(50) Achtstein, A. W.; Schliwa, A.; Prudnikau, A.; Hardzei, M.; Artemyev, M. V.; Thomsen, C.; Woggon, U. Electronic Structure and Exciton-Phonon Interaction in Two-dimensional Colloidal CdSe Nanosheets. *Nano Lett.* **2012**, *12*, 3151–3157.

(51) Norris, D.; Efros, A.; Rosen, M.; Bawendi, M. Size Dependence of Exciton Fine Structure in CdSe Quantum Dots. *Phys. Rev. B* **1996**, *53*, 16347–16354.

(52) Naeem, A.; Masia, F.; Christodoulou, S.; Moreels, I.; Borri, P.; Langbein, W. Giant Exciton Oscillator Strength and Radiatively Limited Dephasing in Two-dimensional Platelets. *Phys. Rev. B* **2015**, *91*, 8–12.

(53) Scott, R.; Achtstein, A. W.; Prudnikau, A. V.; Antanovich, A.; Siebbeles, L. D. A.; Artemyev, M.; Woggon, U. Time-Resolved Stark Spectroscopy in CdSe Nanoplatelets:

Exciton Binding Energy, Polarizability, and Field-Dependent Radiative Rates. *Nano Letters* **2016**, *26*, 6576–6583.

(54) Adachi, S. *Properties of group-IV, III-V and II-VI semiconductors*; WILEY-VCH Verlag, 2005.

(55) Pelton, M. Carrier Dynamics, Optical Gain, and Lasing with Colloidal Quantum Wells. *J. Phys. Chem. C* **2018**, *122*, 10659–10674.

(56) Kunneman, L. T.; Tessier, M. D.; Heuclin, H.; Dubertret, B.; Aulin, Y. V.; Grozema, F. C.; Schins, J. M.; Siebbeles, L. D. A. Bimolecular Auger Recombination of Electron Hole Pairs in Two Dimensional CdSe and CdSe/CdZnS Core/Shell Nanoplatelets. *J. Phys. Chem. Lett.* **2013**, *4*, 3574–3578.

(57) Li, Q.; Lian, T. Area- and Thickness-Dependent Biexciton Auger Recombination in Colloidal CdSe Nanoplatelets: Breaking the "Universal Volume Scaling Law". *Nano Letters* **2017**, *5*, 3152–3158.

(58) Koch, S.; Kira, M.; Khitrova, G.; Gibbs, H. Semiconductor Excitons in New Light. *Nat. Mater.* **2006**, *5*, 523–531.

(59) Lauth, J.; Kulkarni, A.; Spoor, F. C.; Renaud, N.; Grozema, F. C.; Houtepen, A. J.; Schins, J. M.; Kinge, S.; Siebbeles, L. D. Photogeneration and Mobility of Charge Carriers in Atomically Thin Colloidal InSe Nanosheets Probed by Ultrafast Terahertz Spectroscopy. *J. Phys. Chem. Lett.* **2016**, *7*, 4191–4196.

(60) Sie, E. J.; Steinhoff, A.; Gies, C.; Lui, C. H.; Ma, Q.; R?sner, M.; Sch?nhoff, G.; Jahnke, F.; Wehling, T. O.; Lee, Y.-H. et al. Observation of Exciton Redshift-Blueshift Crossover in Monolayer WS_2. *Nano Lett.* **2017**, *17*, 4210–4216.

(61) Sarma, D.; Yang, E. Band-gap Renormalization in Semiconductor Quantum Wells. *Phys. Rev. B* **1990**, *41*, 8288–8294.

(62) Masumoto, Y.; Fluegel, B.; Meissner, K.; Paul, A. Band-Gap Renormalization of Excited CdSe. *J. Crystal Growth* **1992**, *117*, 732–737.

(63) Piermarocchi, C.; Tassone, F.; Savona, V.; Quattropani, A.; Schwendimann, P. Exciton Formation Rates in GaAs/AlxGa1xAs Quantum Wells. *Phys. Rev. B* **1997**, *55*, 1333.

(64) Sippel, P.; Albrecht, W.; Bok, J. C. V. D.; Dijk-moes, R. J. A. V.; Hannappel, T.; Eichberger, R.; Vanmaekelbergh, D. Femtosecond Cooling of Hot Electrons in CdSe Quantum-Well Platelets. *Nano Letters* **2015**, *15*, 2409–2416.

(65) Yoffa, E. J. Screening of Hot-carrier Relaxtion in Highly Photo-Excited Semiconductors. *Phys. Rev. B* **1981**, *23*, 1909–1919.

(66) Semkat, D.; Richter, F.; Kremp, D.; Manzke, G.; Henneberger, K. Ionization Equilibrium in an Excited Semiconductor: Mott Transition versus Bose-Einstein Condensation. *Phys. Rev. B* **2009**, *80*, 155201.

(67) Deng, H. Condensation of Semiconductor Microcavity Exciton Polaritons. *Science* **2002**, *298*, 199–202.

(68) Fraser, M. D.; Höfling, S.; Yamamoto, Y. Physics and Applications of Exciton – Polariton Lasers. *Nat. Mater.* **2016**, *15*, 1049–1052.

Graphical TOC Entry